2013 European Control Conference (ECC)
July 17-19, 2013, Zürich, Switzerland.

Development of an Electromagnet Excited Mass–Pendulum System Modeling and Control Laboratory Experiment — Theory And Test

Kelly R. Austin and John R. Wagner, Ph.D., P.E.

Abstract— **An electromagnet excited mass–pendulum system with attached spring and damper elements is introduced as a senior and graduate level engineering laboratory experiment. This laboratory offers mechanical, electrical, and control engineering challenges to the students. The derivation of the coupled equations of motion is developed using both Newtonian and Lagrangian approaches. The system is pendulum actuated by a powerful electromagnet for which the magnetic force is modeled by a magnetostatic forcing function. Representative numerical and experimental results are presented which validate the mathematical model. Further, the bench top experiment offers hands-on opportunities for the students. The numerical results agree within 2% to 20% of the experiments.**

I. INTRODUCTION

The mass–pendulum system with spring and damper elements is a classical coupled dynamics problem that may be posed to engineering students. The dynamics of the mass-pendulum system, somewhat similar to the suspension spring pendulum interfaces on tower clock mechanisms, offers the challenge of working with a coupled system which is subjected to non-linear motion. The system shares some similarities with the underactuated cart driven inverted pendulum and pendulum driven cart mechanical systems with respective swing-up stabilizing and tracking problems [1][2].

Due to the inertial coupling of the masses, this two mass system also offers an optimization problem in vibration reduction. As a passive tuned mass damper, the pendulum was found to be useful in reducing steady state and low seismic motion [3]. The pendulum has also been researched as an active mass damper against wind and low seismic motion [4]. Both of these have the challenge of working with a system that is subject to non-linear and chaotic motion depending on system damping and forcing frequency [5].

This laboratory experiment incorporates fundamental engineering concepts while working with a nonlinear physical system. Students mathematically model the system by either a direct application of Newton's second law or by use of Lagrange's equations for education purposes. The model is then verified by numerical simulation of the free response of the coupled system which requires analyzing the uncoupled and coupled motion of the masses to determine the system parameter values. Calculating the system parameters from the physical system incorporates sensor integration and calibration, data acquisition, signal processing, and data analysis.

The actuator used is a powerful electromagnet which must be incorporated into the physical system to drive the pendulum based on the real time motion of the coupled system. By mathematically modeling the magnitude of the electromagnet's magnetic force, the forced response of the mass-pendulum mathematical model can be simulated and compared to the forced response of the physical system. With the physical system and validated model, the linear and non-linear motion of the coupled system can be experimentally and analytically evaluated to control the system response.

K. Austin is with Eaton Aerospace Group, Jackson, MS 39206, USA
Professor Wagner is with Clemson University, Clemson, SC 29634, USA

II. MATHEMATICAL MODELS

The coupled mass–pendulum experimental system can be represented by the diagram shown in Fig. 1 where the origin is at point O. The mass M_1 provides a sturdy support assembly for the pendulum of mass M_2. Attached to M_1 is a compression spring with stiffness k. The linear damping coefficient c lumps the damping from the translational spring and the linear bearings acting on M_1. The torsional damping coefficient b results from the rotary bearings that attach the pendulum rod of length R to M_1. The motion of the masses is defined by the horizontal displacement x and the angular displacement θ in terms of the unit vectors $\hat{i}$, $\hat{j}$ and $\hat{k}$, with $\hat{k}$ directed out of the page. The two dimensional motion of the system is confined to the $\hat{i}$-$\hat{j}$ plane.

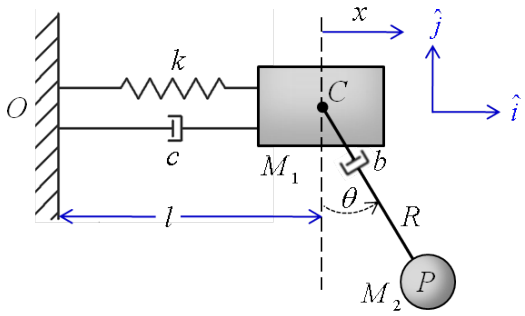

Fig. 1. A mass-pendulum system model with spring and damper elements

To simplify the model, M_1 and M_2 are treated as point masses and air resistance neglected. The spring and rod are considered to be massless. When the spring is un-stretched ($x = 0$) M_1 is at equilibrium. In its equilibrium position where $\theta = 0$, the pendulum is hanging straight down.

A. Direct Method

A direct application of Newton's second law requires defining the accelerations of both masses and identifying the forces associated with their motion.

1) Kinematics of Masses M_1 and M_2: The kinematic equations of M_1 are

$$\vec{r}_c = x\hat{i} \tag{1}$$
$$\vec{v}_c = \dot{\vec{r}}_c = \dot{x}\hat{i} \tag{2}$$
$$\vec{a}_c = \dot{\vec{v}}_c = \ddot{\vec{r}}_c = \ddot{x}\hat{i} \tag{3}$$

where position $\vec{r}_c$, velocity $\vec{v}_c$, and acceleration $\vec{a}_c$ describe the motion of the mass which is constrained to move horizontally. The distance l from O to C at $x = 0$ has been neglected since it does not appear in the derivatives.

The kinematic equations of M_2, which has combined rotational and translational motion, are

$$\vec{r}_p = x\hat{i} + R\sin\theta\hat{i} - R\cos\theta\hat{j} \tag{4}$$
$$\vec{v}_p = \dot{\vec{r}}_p = \dot{x}\hat{i} + R\dot{\theta}\cos\theta\hat{i} + R\dot{\theta}\sin\theta\hat{j} \tag{5}$$
$$\vec{a}_p = \dot{\vec{v}}_p = \ddot{\vec{r}}_p = \ddot{x}\hat{i} + R\left(\ddot{\theta}\cos\theta - \dot{\theta}^2\sin\theta\right)\hat{i} + R\left(\ddot{\theta}\sin\theta + \dot{\theta}^2\cos\theta\right)\hat{j}. \tag{6}$$

2) System Forces: To apply Newton's law to the masses, the system forces must be written as vectors. As the pendulum swings, torsional damping acts on the pendulum. It is assumed that the torsional damping torque is caused by a linear rotary bearing friction force $\vec{F}_b$ which shall be derived.

a) Rotary Bearing Friction: The two rotary bearings were modeled as a single torsional damper with dissipative torque $\vec{\tau}_b = b\dot{\theta}\hat{k}$ [6]. The vector representation of the torque is shown in Fig. 2(a). Equate the expression $\vec{\tau}_b = \vec{R}\times\vec{F}_b = RF_b\hat{k}$ to the dissipative damping acting on M_2, $\vec{\tau}_b = -b\dot{\theta}\hat{k}$, so that the derived force $\vec{F}_b$ acting on M_2 is $F_b = -\frac{b}{R}\dot{\theta}$.

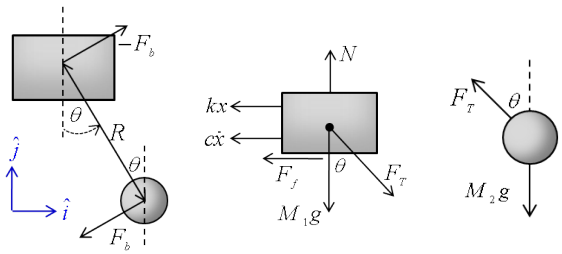

(a) (b) (c)

Fig. 2. Mass-pendulum system with (a) torsional damping τ_b from friction force $\vec{F}_b$ and remaining forces acting on (b) M_1, and (c) M_2

b) Forces Acting on M_1 and M_2: The total forces acting on M_1, shown in Fig. 2(b), are the normal force N, sliding friction F_f, weight, spring force, damping force, tension T, and rotary bearing friction so that

$$\sum\vec{F} = \vec{F}_N + \vec{F}_f + \vec{F}_{M_1} + \vec{F}_k + \vec{F}_c + \vec{F}_T + \vec{F}_b. \tag{7}$$

It is assumed that the sliding friction acting on M_1 is negligible. The total forces acting on M_2, as seen in Fig. 2(c), are the tension, weight, and rotary bearing friction such that

$$\sum\vec{F} = \vec{F}_T + \vec{F}_{M_2} + \vec{F}_b. \tag{8}$$

The force vectors listed in Table I have been resolved into $\hat{i}$ and $\hat{j}$ components.

TABLE I
FORCE VECTORS IN COUPLED SYSTEM

Forces on M_1		Forces on M_2	
$\vec{F}_N$	$N\hat{j}$	$\vec{F}_T$	$T\left(-\sin\theta\hat{i} + \cos\theta\hat{j}\right)$
$\vec{F}_{M_1}$	$-M_1 g\hat{j}$	$\vec{F}_{M_2}$	$-M_2 g\hat{j}$
$\vec{F}_k$	$-kx\hat{i}$	$\vec{F}_b$	$-\frac{b}{R}\dot{\theta}\left(\cos\theta\hat{i} + \sin\theta\hat{j}\right)$
$\vec{F}_c$	$-c\dot{x}\hat{i}$		
$\vec{F}_T$	$T\left(\sin\theta\hat{i} - \cos\theta\hat{j}\right)$		
$\vec{F}_b$	$\frac{b}{R}\dot{\theta}\left(\cos\theta\hat{i} + \sin\theta\hat{j}\right)$		

3) Equations of Motion: Applying Newton's second law of motion to M_1 and M_2 for the external forces given in Table I and the accelerations from (3) and (6) gives

$$N\hat{j} - M_1 g\hat{j} - kx\hat{i} - c\dot{x}\hat{i} + T\left(\sin\theta\hat{i} - \cos\theta\hat{j}\right) + \frac{b}{R}\dot{\theta}\left(\cos\theta\hat{i} + \sin\theta\hat{j}\right) = M_1\ddot{x}\hat{i} \tag{9}$$

$$-M_2 g\hat{j} + T\left(-\sin\theta\hat{i} + \cos\theta\hat{j}\right) - \frac{b}{R}\dot{\theta}\left(\cos\theta\hat{i} + \sin\theta\hat{j}\right) = M_2\Big(\ddot{x}\hat{i} + R\left(\ddot{\theta}\cos\theta - \dot{\theta}^2\sin\theta\right)\hat{i} + R\left(\ddot{\theta}\sin\theta + \dot{\theta}^2\cos\theta\right)\hat{j}\Big). \tag{10}$$

Four simultaneous equations may be realized by considering the $\hat{i}$ and $\hat{j}$ components of these two equations. Ignoring the normal force N, equation allows use of the remaining three simultaneous equations to find the M_1 and M_2 EOMs.

B. Lagrangian Method

Lagrange's method requires finding the Lagrangian function L, which is a function of the system's total kinetic T and potential V energies, energy dissipated due to damping, and any nonconservative forces acting on the system.

1) Lagrangian Function: The motion of each mass can be described in an inertial frame which has an origin at O. In the inertial frame, the position and velocity vectors from O are the same as those given in (1) and (2) for M_1, and (4) and (5) for M_2. The total kinetic energy of the system, which is the sum of the kinetic energies of M_1 and M_2, is found by $T = \frac{1}{2}M_1\left(\vec{v}_c\right)^2 + \frac{1}{2}M_2\left(\vec{v}_p\right)^2$. After substituting (2) and (5), and squaring the velocity vectors, the kinetic energy is $T = \frac{1}{2}M_1\dot{x}^2 + \frac{1}{2}M_2\left(\dot{x}^2 + 2R\dot{x}\dot{\theta}\cos\theta + R^2\dot{\theta}^2\right)$.

The total potential energy in the system due to the position of the spring and M_2 is $V = \frac{1}{2}kx^2 - M_2 gR\cos\theta$. Subtracting the system's potential energy from its kinetic energy gives the Lagrangian function

$$L = T - V = \frac{1}{2}M_1\dot{x}^2 + \frac{1}{2}M_2\dot{x}^2 + M_2R\dot{x}\dot{\theta}\cos\theta + \frac{1}{2}M_2R^2\dot{\theta}^2 - \frac{1}{2}kx^2 + M_2Rg\cos\theta. \quad (11)$$

2) Lagrange's Equations: The equation describing the motion of a generalized coordinate q_i is determined by

$$\frac{d}{dt}\left(\frac{\partial L}{\partial \dot{q}_i}\right) - \frac{\partial L}{\partial q_i} + \frac{\partial D}{\partial \dot{q}_i} = Q_i \quad (i = 1, 2, \cdots) \quad (12)$$

where the Lagrangian L is given in (11), the energy dissipated due to damping is given for the damping coefficient c_i at velocity $\dot{q}_i$ by Rayleigh's dissipation function $D = \frac{1}{2}c_i\dot{q}_i^2$, and the generalized force Q_i encompasses the applied force and any non conservative force such as sliding friction [7].

The EOM for M_1 is found by evaluating (12) for the coordinate $q_1 = x$, where the partial derivatives of (11) are taken with respect to x and $\dot{x}$, and Rayleigh's dissipation function for the damping of x is $D = \frac{1}{2}c\dot{x}^2$. Evaluating (12) for $q_2 = \theta$ gives the dynamics for M_2. The partial derivatives in (11) are taken with respect to θ and $\dot{\theta}$, and $D = \frac{1}{2}b\dot{\theta}^2$ is Rayleigh's dissipation function for the damping in θ.

The EOM for M_1 and M_2 found from Lagrange's method are the same as those found by the direct method, which can be solved for $\ddot{x}$ and $\ddot{\theta}$ respectively to give the EOM for the mass-pendulum system [3][8]

$$\ddot{x} = \frac{1}{M_1 + M_2}\left(M_2R\dot{\theta}^2\sin\theta - M_2R\ddot{\theta}\cos\theta - c\dot{x} - kx\right) \quad (13)$$

$$\ddot{\theta} = \frac{1}{M_2R}\left(-M_2\ddot{x}\cos\theta - M_2g\sin\theta - \frac{b}{R}\dot{\theta}\right). \quad (14)$$

C. Model of Magnetic Force

The magnetic effect of the electromagnet is characterized in terms of magnetic flux density $\vec{B}$. The magnetic flux ϕ is found by integrating the flux density over the surface area that the flux lines pass through. The electromagnet vector field properties can be treated as scalars by viewing the electromagnet and the attracted load, M_2, as a "magnetic circuit" analogous to a resistive electric circuit [9].

It is assumed that the electromagnet is in an electrostatic state powered by the direct current i, and the N coil turns on the tightly wound electromagnet core are linked by the generated magnetic field lines so the magnetomotive force (mmf) becomes $\mathcal{F} = Ni$. The magnetic flux ϕ produced by the mmf follows a mean closed path of length l through each material comprising the magnetic circuit and must be entirely confined in the circuit.

The reluctance $\mathcal{R}$ is a material property defined as l through the material divided by the product of the material's permeability μ and cross sectional area, $\mathcal{R} = l/(\mu A)$. The μ of the material can be factored into the permeability of free space μ_0 and the material's dimensionless relative permeability μ_r. For a magnetostatic measurement, μ is also referred to as the absolute permeability. While μ_0 is a magnetic constant, the relative permeability of a ferromagnetic material depends on the absolute permeability, which depends on the degree to which the material is magnetized [10]. Using an analogy between voltage and magnetomotive force and the definition of $\mathcal{R}$, the mmf becomes

$$\mathcal{F} = Ni = \phi\mathcal{R} = \phi\frac{l}{\mu A} = \phi\frac{l}{\mu_0\mu_r A.} \quad (15)$$

For this approximation of the magnetic force, the magnetic circuit includes a solid core electromagnet and movable load M_2 separated on both sides by equal sized air gaps. The flux mean path is considered to be through the core, a length of l_C, across the air gap, a length of x_g, through the load, a length of l_L, and back across the air gap to the core. The total reluctance is a function of x_g, stated as

$$\mathcal{R}(x_g) = \frac{l_C}{\mu_0\mu_{r_C}A_C} + 2\frac{x_g}{\mu_0\mu_{r_g}A_g} + \frac{l_L}{\mu_0\mu_{r_L}A_L}. \quad (16)$$

where μ_{r_C}, μ_{r_g}, and μ_{r_L} are the relative permeabilities of the core, air gap, and load, and A_C, A_g, and A_L are the cross sectional areas of the core, air gap, and load.

The magnetic force f acting on M_2 can be approximated by considering the work done by the current in the coil and the work required to move M_2 from a position x_g meters away. The derived forcing function is $|f(x_g)| = -\frac{1}{2}\phi^2\frac{d\mathcal{R}(x_g)}{dx_g}$ [9]. The derivative of the reluctance in (16) with respect to x_g is $\frac{d\mathcal{R}(x_g)}{dx_g} = \frac{2}{\mu_0\mu_{r_g}A_g}$, and the flux from (15) is $\phi = \frac{Ni}{\mathcal{R}(x_g)}$. The magnetic force, in Newtons, is calculated from the function

$$|f(x_g)| = -\frac{(Ni)^2}{\mathcal{R}^2(x_g)\mu_0\mu_{r_g}A_g} \quad (17)$$

where $\mathcal{R}(x_g)$ is calculated from (16) for x_g in meters. This forcing function assumes that no fringing of the magnetic flux lines occurs in the air gap, in which the flux lines leaving the core bow out and then come back into the load. The air gap cross sectional area considering fringing A_{g_F} was assumed to be a function of x_g, where $A_{g_F}(x_g) = (\sqrt{A_g} + x_g)^2$ and A_g is the air gap cross sectional area neglecting fringing. Considering this term in (16) and the derivative of this expression with respect to x_g, gives a magnetic force function $|f_F(x_g)|$, which approximates for the fringing of the magnetic flux lines in the air gap, as

$$|f_F(x_g)| = \frac{-(Ni)^2\left(x_g - A_g^{\frac{1}{2}}\right)\left(x_g + A_g^{\frac{1}{2}}\right)^{-3}}{\left(\frac{\frac{2x_g}{\sqrt{\mu_0}}}{\left(x_g + A_g^{\frac{1}{2}}\right)^2} + \frac{l_C\mu_{r_L}A_L + l_L\mu_{r_C}A_C}{\sqrt{\mu_0}\mu_{r_C}A_CA_L}\right)^2}. \quad (18)$$

The displacement x_g of M_2 from the electromagnet and the approximated magnetic force $f(x_g)$ is illustrated in Fig. 3, where the equilibrium position of the system is at the $\hat{x}, \hat{y}$ axes, and the electromagnet is positioned $\pm x_m$ with respect to the $\hat{y}$ -axis. The positive or negative horizontal

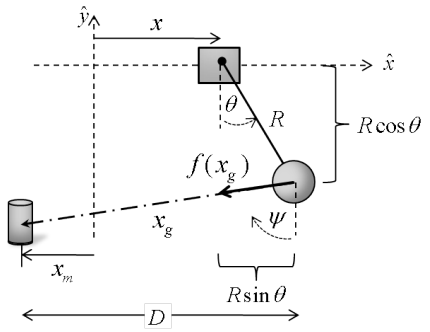

Fig. 3. The magnetic force $f(x_g)$ of the electromagnet, positioned $\pm x_m$ from the equilibrium, acts at angle ψ on the pendulum mass located at a horizontal distance D over the air gap displacement x_g

distance D of M_2 from the electromagnet is found by $D = x + R\sin\theta - x_m$, where the sign of D indicates to which side of the electromagnet M_2 is. From Fig. 3, the magnitude of the displacement x_g is calculated by

$$|x_g| = \sqrt{(x + R\sin\theta - x_m)^2 + (R - R\cos\theta)^2}. \quad (19)$$

The magnetic force produces a torque on the pendulum. This torque is represented as a generalized force in (12) for the coordinate θ as $Q_\theta = \vec{F}_\theta \cdot \frac{\partial \vec{r}_\theta}{\partial \theta}$, where $\vec{r}_\theta$ is given in (4). The magnetic force vector applied to M_2 at an angle ψ from the vertical is $\vec{F}_\theta = -f(x_g)\sin\psi\hat{i} - f(x_g)\cos\psi\hat{j}$. Finding $\psi = \tan^{-1}\left(\frac{D}{R - R\cos\theta}\right)$, the dot product of the force vector and the partial derivative of (4) with respect to θ gives the generalized force acting on M_2 as

$$Q_\theta = -f(x_g)R\sin(\theta + \psi). \quad (20)$$

III. Analysis of System Parameters

By decoupling the motions of M_1 and M_2, the system constants can be analytically and experimentally estimated. The log decrement method was used to estimate the damping ratios of M_1 and M_2, which are assumed to be underdamped.

The general solution of M_1 motion is

$$x(t) = Ae^{-\zeta\omega_n t}\sin\left(\omega_n\sqrt{1-\zeta^2}\,t + \beta\right), \quad (21)$$

with damping ratio $\zeta = c/\left(2\sqrt{M_1 k}\right)$, undamped natural frequency $\omega_n = \sqrt{\frac{k}{M_1}}$, and damped natural frequency $\omega_d = \omega_n\sqrt{1-\zeta^2}$ [11].

Assuming small angle motion,the general solution of the M_2 motion is defined by [11]

$$\theta(t) = Be^{\zeta_p\omega_{n_p}t}\sin\left(\omega_{n_p}\sqrt{1-\zeta_p^2}\,t + \beta_p\right) \quad (22)$$

with undamped natural frequency $\omega_{n_p} = \sqrt{\frac{g}{R}}$ and damping ratio $\zeta_p = \frac{b/(2M_2R^2)}{\sqrt{g/R}}$ [11]. The torsional damping in the pivot point at C causes M_2 to oscillate at a damped natural frequency $\omega_{d_p} = \omega_{n_p}\sqrt{1-\zeta_p^2}$.

For the uncoupled free response of M_1, the logarithmic decrement δ uses the natural logarithm of successive amplitude ratios separated by n periods of length P, [6]

$$\delta = \frac{1}{n}\ln\frac{x(t)}{x(t+nP)}. \quad (23)$$

Using (21) and the definition $P = \frac{2\pi}{\omega_d}$ in this equation, M_1 damping ratio is found as $\zeta = \frac{\delta}{\sqrt{4\pi^2+\delta^2}}$. Using the same procedure, (22) can determine ζ_p for the motion of M_2.

IV. Experimental System

The bench top laboratory experiment shown in Fig. 4 was designed to encourage student interactions with the system. The sensors include a full bridge beam load cell (Omega, part number LCL-010) and a quadrature optical encoder kit (US Digital, part number E2-1024-N-DD-B). The output signal of the load cell is amplified by a strain gauge amplifier (Omega, part number DRC-4710) which also supplies the (5-12)VDC bridge supply to the load cell. The optical encoder kit consists of a 1-inch rotary code wheel with 1024 counts per revolution per channel, read by a HEDS-9100 optical encoder module. The electromagnet, made of 1018 low carbon steel, is wound with 22-AWG magnet wire. The current i is supplied by an external 15VDC power supply controlled by a MOSFET switch using a dSpace controller board DS1103 and a CLP1103 connector panel.

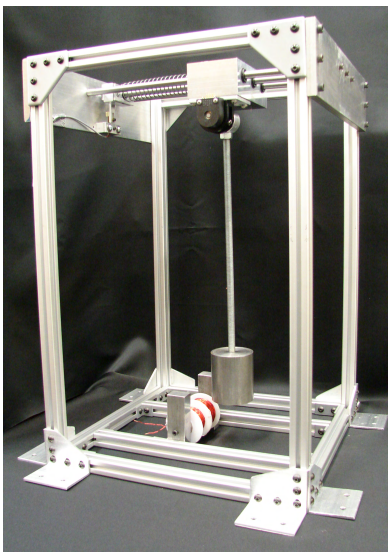

Fig. 4. Mass-pendulum system with integrated sensors and electromagnet

V. Electromagnet Control

The controller should initiate and maintain pendulum motion for general purpose vibration studies. Using the electromagnet to activate the motion of M_2 requires identifying the mass's direction of motion and position with respect to the fixed position of the electromagnet. The electromagnet displacement from the equilibrium position, x_m, can have a maximum value of 11.4cm measured from the electromagnet center. To activate motion, the electromagnet should turn on

when M_2 is swinging toward it, and turn off the moment the pendulum swings past it so that the magnetic field does not slow the motion.

In the physical system, the control logic is incorporated in the Simulink model with dSpace and Control Desk. The control logic is listed in Table II. The logic inputs of the experimental system identify the sets of conditions that must be true for the electromagnet to be activated. The logic inputs of the simulated system identify the conditions that must be true for the positive or negative torque to be calculated for the value of x_g and applied to the system. If the first set of conditions listed for both the experimental and simulated systems is true, the pendulum is approaching the right side of the electromagnet, as shown in Fig. 3. The second set of conditions listed for both system then signals that the pendulum is approaching the left side of the electromagnet.

TABLE II
SYSTEM LOGIC CONDITIONS FOR OUTPUT SIGNAL ACTIVATION

Definition of Logic Input Conditions: u_1 to u_5	
u_1 term	$\text{sgn}\left(\frac{d\lvert x_g\rvert}{dt}\right)$
u_2 term	$\text{sgn}(D)$
u_3 term	$\text{sgn}(\dot{\theta})$
u_4 term	Interval Test, $x_g > \lvert 0.01\text{m}\rvert$
u_5 term	Interval Test, $0.01\text{m} < x_g < 0.10\text{m}$
Logic Inputs Experimental System	**Output**
$u_1 < 0$, $u_2 > 0$, $u_3 < 0$, and u_4=1	On
$u_1 < 0$, $u_2 < 0$, $u_3 > 0$, and u_4=1	On
Logic Inputs Simulated System	**Output**
$u_1 < 0$, $u_2 > 0$, $u_3 < 0$, and u_5=1	$-Q_\theta$
$u_1 < 0$, $u_2 < 0$, $u_3 > 0$, and u_5=1	$+Q_\theta$

VI. NUMERICAL AND EXPERIMENTAL RESULTS

The free and forced responses of the experimental and simulated systems were compared by first determining the experimental system parameters for the simulation. This also required estimating the uncertain electromagnet parameters to derive the magnetic forcing function. All system parameters are listed in Table III.

A. Free Response

The free response of the mass-pendulum system was analyzed for various combinations of initial conditions (ICs) and compared to the free response of (13) and (14) in Matlab for the same ICs. The system free response for which the initial positions of M_1 and M_2 are opposed to each other is shown in Fig. 5(a)–(d). Due to friction, the oscillations in the physical system quickly decrease with all perceptible motion in M_1 ceasing approximately 15sec before M_2 stops oscillating. As can be seen from the plots, by accounting for the friction force ($F_f = \mu_k W \text{sgn}(\dot{x})$ from the linear bearings in M_1, where μ_k is the kinetic friction coefficient and W is the weight) the simulated response gives a good representation of the system motion.

TABLE III
SYSTEM PARAMETERS

Parameter,Variable	Value
Electromagnet Parameters	
Permeability of free space, μ_0	$4\pi \times 10^{-7}$ H/m
Permeability of steel, μ_r	70 ± 10
Permeability of air, μ_{r_g}	1
Mean flux path through core, l_C	0.203m
Mean flux path through load, l_L	5.71×10^{-2}m
Core cross sectional area, A_C	5.07×10^{-4}m^2
Load cross sectional area, A_L	2.74×10^{-3}m^2
Air gap cross sectional area, A_g	1.27×10^{-3}m^2
Turns on electromagnet, N	864turns
Current, i	2.67A
M_1 Parameters	
Mass (including encoder)	0.950kg
Damping ratio, ζ	0.0904 ± 0.0363
Damping coefficient, c	(1.67 ± 0.71)N·s/m
Spring constant, k	(90.1 ± 13.4)N/m
Natural frequency, ω_n	(9.74 ± 0.35)rad/s
Friction coefficient, μ_k	0.015 ± 0.004
M_2 Parameters	
Mass (includes rod mass)	1.363 kg
Rod length, R	0.341 m
Damping ratio, ζ_p	$(1.89\pm0.89)\cdot10^{-4}$
Damping coefficient, b	$(3.18\pm1.54)\cdot10^{-4}$N·m·s
Natural frequency, ω_{n_p}	(5.32 ± 0.01)rad/s

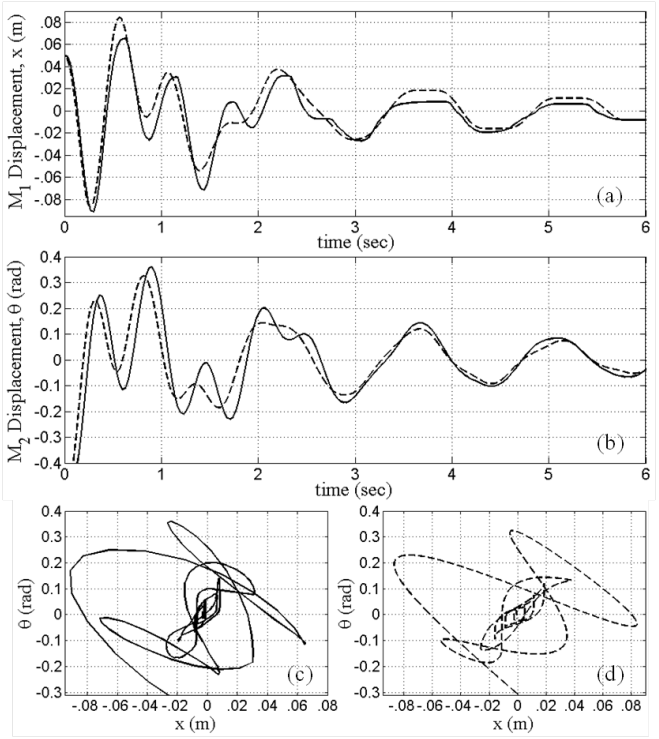

Fig. 5. Comparison of the physical (—) and simulated (- - -) system responses due to initial conditions $\theta_0 = -\pi/6$rad and $x_0 = 0.05$m for (a) M_1, (b) M_2, and (c and d) motion of M_2 with respect to M_1

B. Forced Response

In the experimental system, the forced response was investigated for three positions of the electromagnet, $x_m = (1)\ -4$cm, (2) -7.5cm, and (3) -11.4cm (the response of the system for positive values of x_m placements was found to be similar). To compare the interaction between the masses and the application of the magnetic force, the electromagnet induced motion of M_2 was found, keeping M_1 fixed, and the system's coupled response was found in which M_1 was unconstrained. A summary of the forced system response for the experimental and simulated systems is shown in Tables IV and V. For the case in which M_1 was held stationary, the RMS amplitude and minimum and maximum amplitudes of M_2 are given with its oscillating frequency.

When M_1 is not constrained, the RMS amplitude and the minimum and maximum amplitudes of both M_1 and M_2 were determined for a 10sec sample time after the initial transients died out. Only the oscillating frequency of M_2 is listed since the masses oscillate at the same frequency. For the electromagnet positioned furthest away, the oscillating frequency of M_1 could not be determined.

TABLE IV
EXPERIMENTAL SYSTEM FORCED RESPONSE

M_1 Held Stationary [0–100]sec				
x_m	θ_{rms} (rad)	θ_{min} (rad)	θ_{max} (rad)	ω_{M_2} (rad/s)
1	0.407	-0.825	0.822	5.27
2	0.383	-0.755	0.755	5.27
3	0.237	-0.542	0.542	5.32

M_1 Free to Move [90–100]sec							
x_m	x_{rms} (cm)	x_{min} (cm)	x_{max} (cm)	θ_{rms} (rad)	θ_{min} (rad)	θ_{max} (rad)	ω_{M_2} (rad/s)
1	1.62	-2.94	1.90	0.113	-0.158	0.164	4.50
2	1.22	-1.99	1.32	0.086	-0.144	0.123	4.16
3	0.267	-0.497	-0.155	0.009	-0.017	0.015	5.26

The simulated system response is representative of the response of the physical system up to approximately $\theta = \frac{\pi}{4}$rad for all tests. For Test 1, in which the electromagnet is positioned at -4cm, the physical and the simulated system reach a maximum amplitude of $\frac{\pi}{4}$ in approximately 90sec. The average percent difference between the amplitudes of the two plots for $[0 - 90]$sec is 3.1%. For Test 2, the physical and simulated system reach $\frac{\pi}{4}$ in approximately 100sec, with an average percent difference in their amplitudes of 11.0%. For the electromagnet positioned furthest away, Test 3, M_2 reaches $\frac{\pi}{4}$ in 215sec in the physical response, and 230sec in the simulated. The percent difference between the plots for the first 100sec of motion is 7.7%.

When M_1 is not fixed, per Tables IV and V, the motion of M_1 greatly reduces the amplitude of the pendulum's oscillations for the same force. Starting with a small initial condition, each mass reaches steady state oscillation within five seconds. Compared to the pendulum motion when M_1 is held stationary, when the pivot point of an oscillating mass has allowable motion, the influence of the driving force on the mass is damped. The motion of M_1, which is constrained by the attached spring, effectively limits the motion of M_2. Thus a much larger force would be required to increase the oscillating amplitudes of the masses.

TABLE V
SIMULATED SYSTEM FORCED RESPONSE

M_1 Held Stationary [0–100]sec				
x_m	θ_{rms} (rad)	θ_{min} (rad)	θ_{max} (rad)	ω_{M_2} (rad/s)
1	0.400	-0.809	0.806	5.23
2	0.369	-0.766	0.768	5.27
3	0.244	-0.528	0.525	5.32

M_1 Free to Move [90–100]sec							
x_m	x_{rms} (cm)	x_{min} (cm)	x_{max} (cm)	θ_{rms} (rad)	θ_{min} (rad)	θ_{max} (rad)	ω_{M_2} (rad/s)
1	1.88	-3.05	1.99	0.0883	-0.139	0.132	4.22
2	1.42	-2.20	2.13	0.0943	-0.179	0.105	3.84
3	0.0228	-0.0195	0.0312	0.0202	-0.0293	0.0278	5.37

VII. CONCLUSION

This mass–pendulum laboratory experiment provides engineering students an opportunity to model and investigate a coupled dynamics problem. In using a physical system to validate a mathematical model, students gain experience in simulating a non-linear model, determining physical parameter values, and acquiring and analyzing data.

REFERENCES

[1] K. Sakurama, S. Hara, and K. Nakano, "Swing-up Stabilization Control of a Cart–Pendulum System via Energy Control and Controlled Lagrangian Methods", *in Electrical Engineering in Japan*, vol. 160, No. 4, 2007, pp. 617-623.

[2] H. Yu, Y. Liu, and T. Yang, "Closed-Loop Tracking Control of A Pendulum–Driven Cart–Pole Underactuated System", *Proc. IMechE*, vol. 222 Part I, 2008, pp. 109-125.

[3] E. Matta and A. De Stefano, "Seismic Performance of Pendulum and Translational Roof-garden TMDs", *in Mechanical Systems and Signal Processing*, vol. 23, No. 3, 2009, pp. 908-921.

[4] N. Abe, "Passive and Active Switching Vibration Control with Pendulum Type Damper", *in Proceedings of 2004 IEEE Conference on Control Applications* Taipei, Taiwan, 2004, pp. 1034-1042.

[5] Y. Song, H. Sato, Y. Iwata, and T. Komatsuzaki, "The Response of A Dynamic Vibration Absorber System with A Parametrically Excited Pendulum", *Journal of Sound and Vibration*, 2003, pp. 747-759.

[6] W. J. Palm III, *System Dynamics*, McGraw-Hill, New York, NY; 2005.

[7] D. T. Greenwood, *Principles of Dynamics*, Prentice Hall, Englewood Cliffs, NJ; 1988.

[8] J. H. Williams, Jr., *Fundamentals of Applied Dynamics*, John Wiley and Sons, Inc., New York, NY; 1996.

[9] G. Rizzoni, *Principles and Applications of Electrical Engineering*, 5th Ed., McGraw-Hill, New York, NY; 2007.

[10] D. G. Fink and H. W. Beaty, *Standard Handbook for Electrical Engineers*, 13th Ed., McGraw-Hill, New York, NY; 1993.

[11] D. G. Zill and M. R. Cullen, *Advanced Engineering Mathematics*, 2nd Ed., Jones and Bartlett Publishers, Inc., Boston, MA; 2000.